Journal of Marine Science and Technology

Volume 24 | Issue 5 Article 7

MECHNICAL STRENGTH AND DURABILITY OF ALKALI-ACTIVATED FLY ASH/SLAG CONCRETE

Maochieh Chi
Dept. of Fire Science, WuFeng University, Chiayi County, Taiwan, R.O.C., jackchi@wfu.edu.tw

Journal of Marine Science and Technology, Vol. 24, No. 5, pp. 958-967 (2016)
DOI: 10.6119/JMST-016-0603-1

MECHNICAL STRENGTH AND DURABILITY OF ALKALI-ACTIVATED FLY ASH/SLAG CONCRETE

Maochieh Chi

Key words: mechanical strength, durability, alkali-activated fly ash/slag (AAFS) fly ash/slag ratio, sodium oxide, activator modulus ratio.

ABSTRACT

This study investigated the mechanical strength and durability of alkali-activated binders composed of blends of fly ash (FA) and ground granulated blast furnace slag. Five samples with FA/slag ratios of 100/0, 75/25, 50/50, 25/75, and 0/100 by mass were employed to prepare alkali-activated FA/slag (AAFS) concrete. Sodium oxide (Na_2O) concentrations of 6% and 8% of binder weight and activator modulus ratios (mass ratio of SiO_2 to Na_2O) of 0.8, 1.0, and 1.23 were used to prepare alkaline activators. Test results revealed that higher slag contents, Na_2O concentrations, and activator modulus ratios increased the compressive strength and splitting tensile strength of AAFS concrete. The total charge passed through AAFS concrete was between 2500 and 4000 C, higher than that passed through reference ordinary Portland cement (OPC) concrete. However, AAFS concrete demonstrated higher performance than that of OPC concrete when exposed to sulfate. According to scanning electron microscopy observations, the main hydration products of AAFS concrete were amorphous alkaline aluminosilicate and low-crystalline calcium silicate hydrate gel. As the slag content increased, the amount of C-S-H gel increased and that of A-S-H gel decreased. According to the results, 100% slag-based AAFS concrete with a Na_2O concentration of 8% and activator modulus ratio of 1.23 offers superior performance.

I. INTRODUCTION

Alkali-activated binders have attracted considerable attention because of their excellent mechanical properties, durability, and environmental benefits (Palomo et al., 1999; Roy, 1999; Fernández-Jiménez et al., 2006; Oh et al., 2010; Juengera et al., 2011). Fly ash (FA) and ground granulated blast furnace slag (GGBFS) are the most frequently used raw materials in the production of alkali-activated binders. Their activation has been studied extensively over the past decades (Bakharev et al., 1999; Palomo et al., 1999; Roy, 1999; Fernández-Jiménez et al., 2006; Gruskovnjak et al., 2006; Kumar et al., 2009). The synthesis conditions of alkali-activated FA and slag are similar, but their reaction products are different (Li et al., 2010; Chi and Huang, 2013; Lee and Lee, 2015). The main reaction product of alkali-activated FA is amorphous aluminosilicate gel (A-S-H gel) (Komljenović et al., 2010; Criado et al., 2012; Jun and Oh, 2014), whereas that of alkali-activated slag is calcium silicate hydrate gel (C-S-H gel) (Neto et al., 2008; Bernal et al., 2011; Chi, 2012; Chi and Huang, 2012). The major features of alkali-activated FA are low shrinkage, high acid resistance, and high heat resistance (Lee and Deventer, 2002; Fernández-Jiménez et al., 2006), whereas those of alkali-activated slag are rapid setting, high strength, and high fire resistance (Neto et al., 2008; Bernal et al., 2011; Shi et al., 2011; Yang et al., 2011; Chi, 2012). Many previous studies have investigated either alkali-activated FA or slag, but only a few studies have investigated their combined use.

Blended FA and slag binders are attracting increasing attention because of the favorable combinations of mechanical strength and durability that can be obtained through the co-existence of the two gel types (Zhao et al., 2007; Shi et al., 2011; Lee and Lee, 2013; Ismail et al., 2014; Lee et al., 2014; Gao et al., 2015; Marjanović et al., 2015). Zhao et al. (2007) reported that the compressive strength of alkali-activated FA/slag (AAFS) mortars reached up to 49 MPa at 28 days. Lee and Lee (2013) investigated the mechanical and setting properties of AAFS concrete and found that a slag content of 15%-20% of total binder by weight in AAFS mixtures is suitable, considering the setting time and compressive strength of AAFS concrete; they also revealed that the modulus of elasticity and splitting tensile strength of AAFS concrete were slightly lower than those of ordinary Portland cement (OPC) concrete. Moreover, Lee et al. (2014) reported that higher sodium silicate and slag contents in a mixture caused more chemical, autogenous, and drying shrinkage, but led to higher compressive strength. Marjanović et al. (2015) indicated that the compressive strength depended on the composition of FA/slag blends and the water-to-binder ratio. AAFS mortar with an FA/slag mass ratio of 25/75, activator modulus ratio of 1.0,

Paper submitted 10/16/15; revised 01/04/16; accepted 06/03/16. Author for correspondence: Maochieh Chi (e-mail: jackchi@wfu.edu.tw).
Dept. of Fire Science, WuFeng University, Chiayi County, Taiwan, R.O.C.

Table 1. Physical properties of OPC, FA and GGBFS.

Physical properties	OPC	FA	GGBFS
Specific gravity	3.16	2.06	2.88
Specific surface area (m^2/g)	0.352	0.405	0.435

Table 2. Chemical compositions of OPC, FA and GGBFS.

Chemical compositions (%)	OPC	FA	GGBFS
Calcium oxide, CaO	63.56	1.94	40.67
Silicon dioxide, SiO_2	21.04	56.66	34.58
Aluminum oxide, Al_2O_3	5.46	23.97	13.69
Ferric oxide, Fe_2O_3	2.98	7.56	0.44
Sulfur trioxide, SO_3	2.01	0.57	0.56
Sodium oxide, Na_2O	0.32	0.33	0.15
Potassium oxide, K_2O	0.70	0.8	0.32
Magnesium oxide, MgO	2.52	1.34	7.05
Loss on ignition, L.O.I.	1.38	2.76	1.13
Others	0.03	4.07	1.41

and sodium oxide (Na_2O) concentration of 10% demonstrated optimum physical-mechanical characteristics. On the basis of compressive strength test results, Gao et al. (2015) showed that the optimum activator modulus changed with the slag/FA mass ratio, and higher slag/FA mass ratios favored higher activator moduli. According to Yang et al. (2012a), incorporating partial slag into FA improved the compressive strength of geopolymer binders and affected the reaction mechanism controlling the formation of the main binding gel.

Despite these previous studies on alkali-activated blended FA and slag binders, the exact nature of gel coexistence regimes and phenomena are not adequately understood yet. The chemical composition of alkali activation remains a subject of discussion in the scientific literature, and it depends on the physico-chemical nature of raw materials, nature and quantity of activators, and curing conditions (Bakharev et al., 1999; Collins and Sanjayan, 1999; Collins and Sanjayan, 2000; Bernal et al., 2010). Therefore, the current study investigated the mechanical strength and durability of AAFS concrete by conducting compressive strength, splitting tensile strength, rapid chloride penetration, and sulfate attack resistance tests, in addition to scanning electron microscopy (SEM) observations.

II. EXPERIMENTAL

1. Materials

The main binder materials used in this study were Class F FA, according to ASTM C618 (2012), obtained from the Mailiao Six Light Naphtha Cracker Plant located in Yunlin county, Taiwan, and GGBFS supplied by CHC Resources Corporation, Taiwan. OPC type I conforming to ASTM C150 (2012) was used as a reference binder material. The physical properties and chemical compositions of the aforementioned materials are listed in Tables 1 and 2, respectively. The most used alkaline activators are a mixture of NaOH and sodium silicate ($Na_2O.\ \gamma SiO_2$) (Yang et al., 2008). In this study, alkaline activation of FA and GGBFS was performed using NaOH pellets with a density of 2130 kg/m^3 and a sodium silicate solution ($Na_2O.\ \gamma SiO_2.nH_2O$) consisting of 29.2% SiO_2, 14.8% Na_2O, and 56.0% H_2O by mass. Furthermore, Na_2SiO_3 and NaOH solutions were prepared 1 day before they were used. Crushed gravel and river sand were used as coarse and fine aggregates for preparing concrete. The coarse aggregate had a density of 2610 kg/m^3, a fineness modulus of 6.26, and an absorption of 1.36%, whereas the fine aggregate had a density of 2540 kg/m^3, a fineness modulus of 3.1, and an absorption of 2%.

2. Mix Design and Specimen Preparation

At the mix design stage, the liquid/binder ratio was maintained at 0.5 in all samples. OPC concrete and AAFS concrete mixes with binder at a proportion of 440 kg/m^3, according to ASTM C 192 (2014), were designed. Studies have shown that Na_2O concentration and activator modulus ratio considerably influence the mechanical properties and durability of AAFS concrete. Moreover, the binding mechanism and properties of AAFS mortars with a modulus ratio (mass ratio of SiO_2 to Na_2O) of 1.0 improved with increasing Na_2O concentration (Chi and Huang, 2013). Hence, two Na_2O concentration levels of 6% and 8%, expressed as percentages of the weight of cementitious materials in mixtures, and three activator modulus ratio (mass ratio of SiO_2 to Na_2O) levels of 0.8, 1.0, and 1.23 (with symbols L, M, and H) were used as alkaline activators to alkali-activate samples with various FA/slag ratios. FA/slag ratios of 100/0, 75/25, 50/50, 25/75, and 0/100 by mass were employed (denoted by A to E, respectively). OPC concrete and AAFS concrete with FA/slag activated by alkaline solutions were prepared, and detailed information about the mixing proportions is provided in Table 3. Phosphoric acid was used as a retarder to avoid the quick-setting problem of AAFS. All samples were prepared in a mechanical mixer. First, solid materials were added into the mixer. Subsequently, water and liquid sodium silicate were added to the mixture. All AAFS concrete specimens were mixed with phosphoric acid, acting as a setting retarder, to extend the initial setting time. The mixture was mixed for 2 min at a medium speed. The fresh concrete was then poured into cylindrical steel molds measuring 100 mm in diameter and 200 mm in height. The concrete-containing cylinders were vibrated for 1 min; subsequently, they were covered with a plastic film on top and left to set for 24 h. Finally, all samples were demolded and shifted to a curing room with 80% RH and a temperature of 25°C. The samples were stored in the curing room until they were tested.

3. Methods

1) Compressive Strength Tests

Compressive strength tests were conducted on the specimens according to ASTM C39 (2014). Cylindrical specimens ($\phi 100 \times$

Table 3. Mix proportions of OPC and AAFS concrete.

Mix No.	Water (kg/m^3)	Cement (kg/m^3)	FA (kg/m^3)	GGBFS (kg/m^3)	Fine Aggregate (kg/m^3)	Coarse Aggregate (kg/m^3)	Na_2SiO_3 (kg/m^3)	NaOH (kg/m^3)	Phosphoric acid (kg/m^3)
OPC	220	440	0	0	597	954	0	0	0
AM6	147	193	440	0	554	885	87.1	18.6	12.3
AL8	139	184	440	0	554	885	92.9	28.9	11.6
AM8	126	172	440	0	554	885	116.2	24.7	10.5
AH8	112	157	440	0	554	885	142.9	20.0	9.3
BM6	147	193	330	110	562	897	87.1	18.6	12.3
BL8	139	185	330	110	562	897	92.9	28.9	11.6
BM8	126	172	330	110	562	897	116.2	24.7	10.5
BH8	112	158	330	110	562	897	142.9	20.0	9.3
CM6	147	194	220	220	569	910	87.1	18.6	12.3
CL8	139	186	220	220	569	910	92.9	28.9	11.6
CM8	126	173	220	220	569	910	116.2	24.7	10.5
CH8	112	158	220	220	569	910	142.9	20.0	9.3
DM6	147	194	110	330	577	922	87.1	18.6	12.3
DL8	139	186	110	330	577	922	92.9	28.9	11.6
DM8	126	174	110	330	577	922	116.2	24.7	10.5
DH8	112	159	110	330	577	922	142.9	20.0	9.3
EM6	147	195	0	440	585	934	87.1	18.6	12.3
EL8	139	187	0	440	585	934	92.9	28.9	11.6
EM8	126	174	0	440	585	934	116.2	24.7	10.5
EH8	112	160	0	440	585	934	142.9	20.0	9.3

200 mm) of each mixture were prepared, and three specimens of each mixture were tested at 3, 7, 14, and 28 days to determine the average compressive strength.

2) Splitting Tensile Tests

Splitting tensile strength tests were performed on the specimens according to ASTM C496 (2011). Cylindrical specimens (ϕ100 × 200 mm) of each mixture were prepared, and three specimens of each mixture were tested at 3, 7, 14, and 28 days to determine the average splitting tensile strength.

3) Rapid Chloride Penetration Test

Rapid chloride penetration tests (RCPTs) were conducted on the specimens of each mixture in accordance with ASTMC1202 (2012). At 28 days, two specimens measuring 100 mm in diameter and 50 mm in thickness, and conditioned according to the standard were subjected to a potential of 60 ± 0.1 V for 6 h. The total charge passed through the concrete specimens was determined and used to evaluate the chloride permeability of each concrete mixture. ASTM C1202 recommends the qualitative criterion "chloride ion penetrability" according to the range of the total charge passed, as summarized in Table 4.

4) Sulfate Attack Resistance Tests

The sulfate attack resistance of the concrete samples was evaluated according to ASTM C88 (2013). After casting, the demolded specimens were immersed in saturated sodium sulfate solution (pH = 8.7) for 24 h. The specimens were then dried in an oven at 105 ± 5°C for 24 h. This test cycle was repeated five times to investigate the effects of sulfate attack in terms of weight loss and compressive strength reduction. Three cylinders were tested for each record. The weight loss and compressive strength reduction were calculated as follows:

Table 4. Chloride-ion penetrability based on charge passed recommended in ASTM C 1202 ("ASTM C 1202. Standard Test Method for Electrical Indication of Concrete's Ability to Resist Chloride Ion Penetration. American Society for Testing and Materials," 2012).

Charge passed	Chloride-ion penetrability
larger 4000	High
2000 ~ 4000	Moderate
1000 ~ 2000	Low
100 ~ 1000	Very low
smaller 100	Negligible

$$\text{Weight Loss: } \mathrm{WL}(\%) = [(W_0 - W_1)/W_0] \times 100 \quad (1)$$

Compressive Strength Reduction:

$$\mathrm{RCS}(\%) = [(S_0 - S_1)/S_0] \times 100 \quad (2)$$

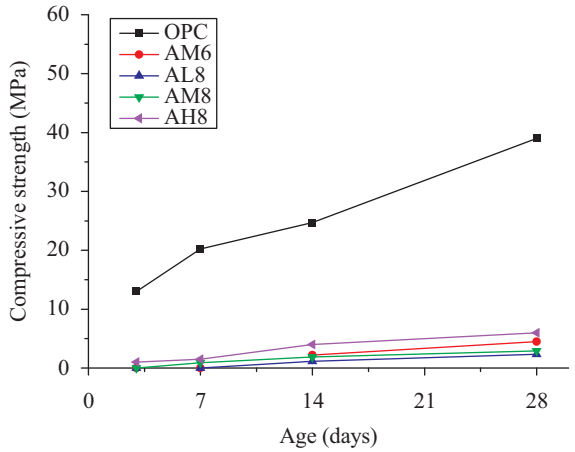

Fig. 1. Compressive strength development of OPC and alkali-activated 100% fly ash-based concrete specimens with different sodium oxide concentrations and activator modulus ratios The frame structure of the transmitted bit stream.

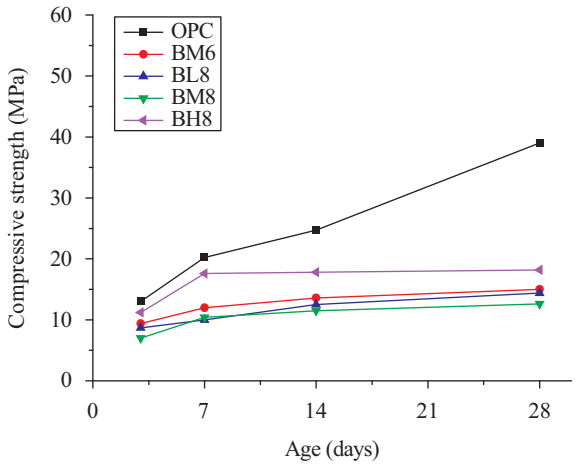

Fig. 2. Compressive strength development of OPC and AAFS with fly ash/slag ratio of 75/25 concrete specimens with different sodium oxide concentrations and activator modulus ratios.

where W_0 is the weight of dried specimens before the test, W_1 is the weight of dried specimens after the test, S_0 is the compressive strength of the specimen cured for 28 days, and S_1 is the compressive strength of the specimen cured in the sulfate solution.

5) Scanning Electron Microscopy

Specimens measuring 10 mm × 10 mm × 3 mm were prepared from the ϕ100 × 200 mm cylindrical specimens at 28 days. Before the execution of SEM analyses, representative specimens were subjected to air drying followed by resin impregnation. The impregnated specimens were ground and softly polished with sandpaper down to 0.25 μm. SEM analyses were performed using a HITACHI S-4100 microscope equipped with an energy-dispersive spectrometer (EDS).

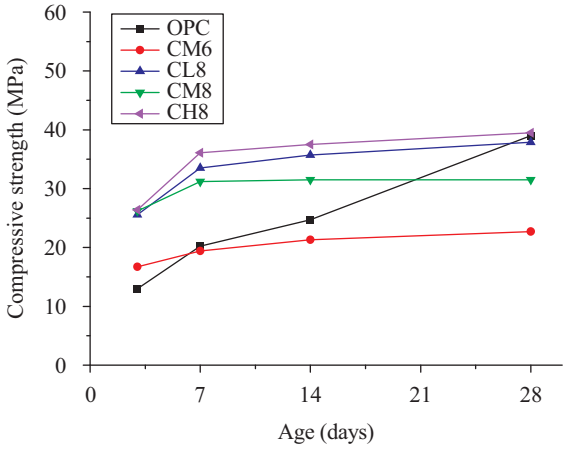

Fig. 3. Compressive strength development of OPC and AAFS with fly ash/slag ratio of 50/50 concrete specimens with different sodium oxide concentrations and activator modulus ratios.

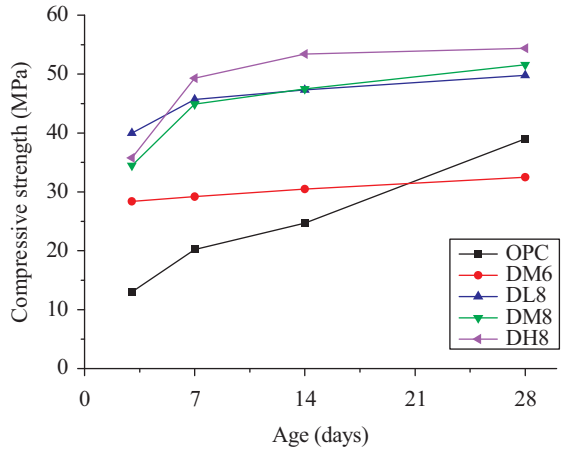

Fig. 4. Compressive strength development of OPC and AAFS with fly ash/slag ratio of 25/75 concrete specimens with different sodium oxide concentrations and activator modulus ratios.

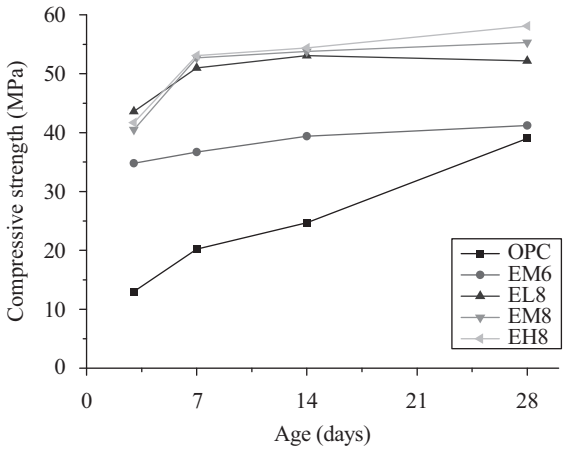

Fig. 5. Compressive strength development of OPC and alkali-activated 100% slag-based concrete specimens with different sodium oxide concentrations and activator modulus ratios.

III. RESULTS AND DISCUSSION

1. Compressive Strength

Figs. 1-5 show the compressive strengths of AAFS specimens of various FA/slag ratios and OPC concrete specimens of different Na_2O concentrations and activator modulus ratios. Most of the compressive strength development of AAFS concrete occurred during the first 7 days, followed by a lower rate of compressive strength development at later ages, whereas the compressive strength development of OPC concrete increased continuously during the 28 days. These results indicate that the FA/slag ratio, Na_2O concentration, and activator modulus ratio considerably influence compressive strength. The compressive strengths of all AAFS concrete specimens increased as the FA/slag ratio decreased. FA-based binders reacted slower than alkali-activated-slag pastes did (Fernández-Jimenez et al., 2006; Duxson et al., 2007; Ismail et al., 2014). Moreover, 100% FA-based concrete specimens without slag exhibited extremely low compressive strength development during the curing time. In this study, compressive strength was improved by the addition of slag. For a constant activator modulus ratio or Na_2O concentration, higher compressive strengths, even exceeding that of OPC concrete, were observed in AAFS concrete specimens with higher slag contents in all cases, as reported in previous studies as well (Kumar et al., 2009; Lee et al., 2014; Gao et al., 2015). Therefore, AAFS concrete specimens with 100% slag-based binder without FA demonstrated the highest compressive strengths, regardless of the activator modulus ratio and Na_2O concentration levels. The increase in compressive strength with the addition of slag, which contains a large amount of CaO, is because the presence of CaO improves the strength of the geopolymer by forming an amorphously structured Ca-Al-Si gel (Lee and Lee, 2013).

Na_2O concentration levels and activator modulus ratios have different effects on the compressive strength of AAFS concrete specimens characterized by different FA/slag ratios. The compressive strength of the AAFS concrete specimens with FA/slag ratios of 100/0 and 75/25 decreased as the Na_2O concentration increased. However, no obvious reduction in compressive strength was observed as the Na_2O concentration increased from 6% to 8%. In general, a higher Na_2O concentration has a positive effect on compressive strength. The reason for the reduction in compressive strength is not clearly understood; it could be due to the variability in the compressive strength test because the AAFS concrete specimens with FA/slag ratios of 100/0 and 75/25 showed extremely low compressive strength development compared with the OPC concrete specimens during curing. When the FA/slag ratio is equal to or greater than 50/50, the compressive strength of AAFS concrete specimens increases with the Na_2O concentration. Higher Na_2O concentrations appear to be more appropriate as an activation condition to increase the dissolution of both FA and slag, which can engender a reaction to form high-strength calcium substituted sodium aluminosilicate (C,N)-A-S-H binding phases, as reported in previous studies (Puertas et al., 2000; M. Chi and Huang, 2012; Chi and Huang, 2013). In addition, the compressive strength of the AAFS concrete specimens increased with the activator modulus ratio. In the case of the samples with an FA/slag ratio of 25/75, the highest compressive strength of 54.4 MPa was observed at an activator modulus ratio of 1.23; the compressive strength then decreased with the activator modulus ratio, reaching its lowest value of 49.8 MPa at an activator modulus ratio of 0.8. A relatively high activator modulus ratio positively influences the dissolution of calcium and the formation of C-A-S-H gels (Phair et al., 2000), thus resulting in higher compressive strength.

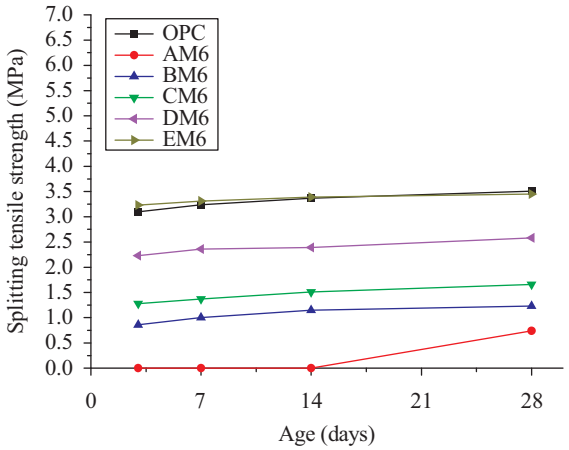

Fig. 6. Splitting tensile strength development of OPC and different fly ash-to-slag ratio AAFS concrete specimens with sodium oxide concentration of 6% and activator modulus ratio of 1.0.

According to the test results, most of the AAFS concrete specimens showed increased compressive strength over the first 7 days of curing, whereas the OPC concrete specimen achieved the same compressive strength over 28 days of curing. The compressive strength of AAFS concrete at 28 days increased with the slag content. The higher the FA/slag ratio was, the lower was the compressive strength. Moreover, higher activator modulus ratios and Na_2O concentration levels resulted in more favorable development of compressive strength in AAFS concrete.

2. Splitting Tensile Strength

Figs. 6-9 illustrate the splitting tensile strength of the OPC sample and AAFS concrete specimens with different FA/slag ratios, Na_2O concentrations, and activator modulus ratios at 3, 7, 14, and 28 days of curing. As shown in this figure, the splitting tensile strength of AAFS concrete increased slightly during the first 7 days, followed by an increase at a much lower rate at later ages, whereas the splitting tensile strength of OPC concrete increased continuously over the 28 days of curing. For the AAFS concrete specimens, the trend of splitting tensile strength is similar to that of compressive strength. The splitting tensile strength of the AAFS concrete specimens with 100% FA and no slag was extremely low (almost 0), and this is attributed to the relatively low reactivity of FA at ambient temperature (Duxson and Provis, 2008). The splitting tensile

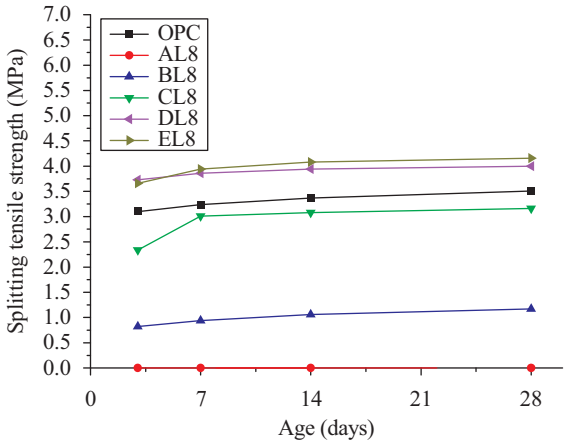

Fig. 7. Splitting tensile strength development of OPC and different fly ash-to-slag ratio AAFS concrete specimens with sodium oxide concentration of 8% and activator modulus ratio of 0.8.

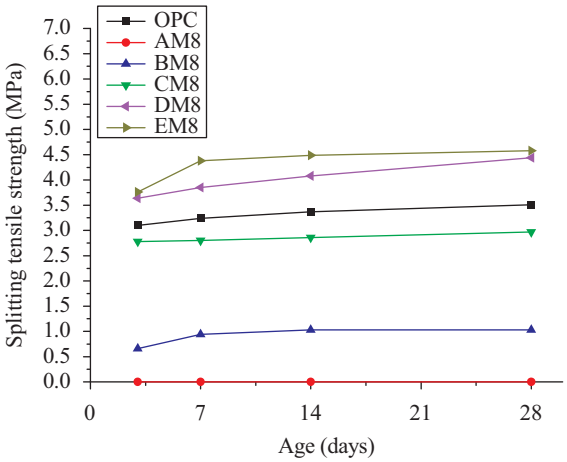

Fig. 8. Splitting tensile strength development of OPC and different fly ash-to-slag ratio AAFS concrete specimens with sodium oxide concentration of 8% and activator modulus ratio of 1.0.

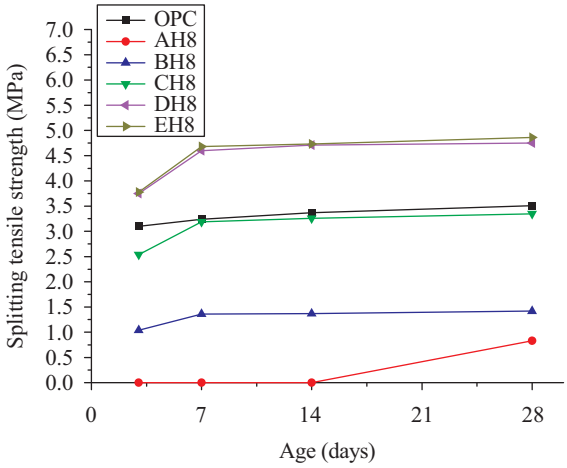

Fig. 9. Splitting tensile strength development of OPC and different fly ash-to-slag ratio AAFS concrete specimens with sodium oxide concentration of 8% and activator modulus ratio of 1.23.

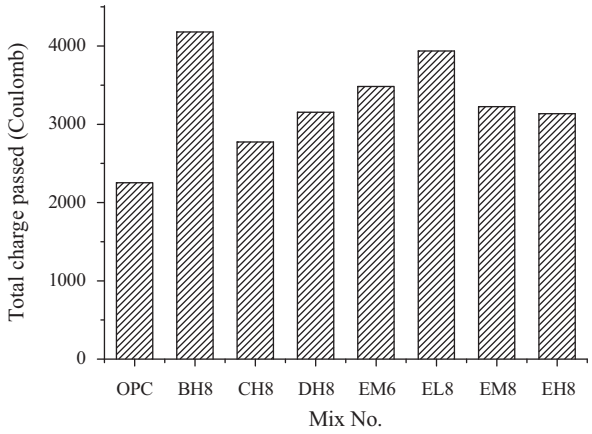

Fig. 10. Total charge passed of OPC and different fly ash-to-slag ratio AAFS concrete specimens with different sodium oxide concentrations and activator modulus ratios.

strengths of all the AAFS concrete specimens increased as the FA/slag ratio decreased. As the amount of slag increased, the splitting tensile strength increased because of the formation of C-A-S-H gel in the AAFS concrete specimens (Yang et al., 2012b). When the AAFS concrete specimens were activated by alkali solution with a Na_2O concentration of 6% and an activator modulus ratio of 1.0, their splitting tensile strengths were lower than those of the OPC concrete specimens at all ages, with the exception of the AAFS concrete specimens containing 100% slag-based binder and no FA (Fig. 6).

When the AAFS concrete specimens were activated by alkali solution with a Na_2O concentration of 8%, the splitting tensile strengths of the specimens characterized by FA/slag ratios of 25/75 and 0/100 were higher than those of the OPC concrete specimens at all ages and increased with the activator modulus ratio (Figs. 7-9). This indicates that the splitting tensile strength development of AAFS concrete specimens is related to the FA/slag ratio, Na_2O concentration, and activator modulus ratio.

3. Rapid Chloride Penetration Test

RCPT is a method of monitoring the amount of electrical current passing through a cylindrical concrete specimen in the first 6 h, and the resistance of the concrete specimen to chloride ion penetration is assessed by the total charge passed in 6 h. Five levels of chloride-ion penetrability are identified to classify the charge passed, namely high, moderate, low, very low, and negligible. The values of total charge passed obtained from RCPTs conducted on the AAFS and OPC concrete specimens at 28 days are presented in Fig. 10. The total charge passed values obtained for the AAFS concrete specimens were higher than that of the reference OPC concrete specimen, which is in agreement with the findings of previous research (Zhu et al., 2014). For the AAFS concrete specimens with a

Na_2O concentration of 8% and activator modulus ratio of 1.23, the CH8 concrete specimen had the least total charge passed value, followed the DH8 and EH8 concrete specimens. The BH8 concrete specimen had the highest total charge passed value, twice as much as that of the OPC concrete specimen. This indicates that the total charge passed through the AAFS concrete specimens increased as the slag content exceeded 50%. For the 100% slag-based AAFS concrete specimens without FA, the total charge passed value decreased as the activator modulus ratio increased. The AAFS concrete specimens could be ordered as EL8 > EM8 > EH8. In addition, the total charge passed through the EM6 concrete specimens was slightly higher than that through the EM8 concrete specimens. Except for the BH8 concrete specimen, the total charge passed through the AAFS concrete specimens ranged between 2500 and 4000 C, corresponding to moderate permeability to chloride ions, according to ASTM C1202 classifications of the testing method.

The total charge passed through the AAFS concrete specimens in this study is slightly higher than that in a previous study (Bernal et al., 2011). In AAFS binders, studies have identified that pore solutions contain high concentrations of ionic species, mainly Na^+ and OH^-, which influence the test results (Gruskovnjak et al., 2006; Lloyd et al., 2010; M. Chi, 2012). Every Na^+ in the pore solution counter-diffuses as the Cl^- ions are electrically driven through the pore network by a forced electrical field gradient, leading to an increase in the total charge passed (Bernal et al., 2012). Therefore, the total charge passed, as measured in the AAFS concrete specimens, could be higher than that corresponding to the actual chloride permeability (Bernal et al., 2011). In addition, Zhu et al. (2014) indicated that porosity and tortuosity are the two most significant factors affecting chloride-ion penetration in alkali-activated FA concrete. Hence, further analysis of the accurate applicability of RCPT to AAFS concrete specimens is required.

4. Sulfate Attack Resistance

Sulfate attack on OPC concrete is regarded as a chemical reaction of sulfate ions, acting as the aggressive substance, with the aluminate component of hardened cement paste (Bakharev et al., 2002). The reactions of such substances, alumina-bearing hydration products, or unhydrated tricalcium aluminate with calcium hydroxide produces ettringite and gypsum, which leads to the expansion and cracking of OPC concrete (Monteiro and Kurtis, 2003; Veiga and Gastaldini, 2012; Komljenović et al., 2013). The results of tests conducted to evaluate the sulfate attack resistance of OPC and AAFS concrete specimens are summarized in Table 5. The results revealed that the weight loss and compressive strength reduction of OPC concrete increased by 2.5% and 20.18%, respectively, which is consistent with the results of a previous study (Bakharev et al., 2002). This indicates that the nature of sulfate attack has a slight negative effect on the evolution of the weight and compressive strength of OPC concrete. Furthermore, the results showed slight reductions in the weight and compressive strength of AAFS concrete, excluding the 100% FA-based concrete specimens without slag. The weight and compressive strength of the AAFS concrete specimens with FA/slag increased by 0.5%-2.3% and 2.6%-20%, respectively, after the sulfate attack resistance test. Generally, the AAFS concrete specimens had smaller pores and exhibited significantly higher resistance to sulfate attack, compared with OPC concrete (Veiga and Gastaldini, 2012; Komljenović et al., 2013). The increase in weight of AAFS concrete in sulfate medium was probably due to the formation of reaction products between AAFS concrete and the sulfate medium. Hence, the porosity of AAFS concrete decreased, and its compressive strength increased. In summary, AAFS concrete demonstrated higher performance than did OPC concrete when exposed to sulfate attack. In addition, AAFS concrete showed a certain increase in strength with time in the sodium sulfate solution. However, no obvious regular trends in the weight loss and compressive strength reduction of the AAFS concrete specimens were observed. Therefore, a longer test period and further analysis of the accurate applicability of sulfate attack resistance to AAFS concrete are required.

Table 5. Sulphate attack resistance of OPC and AAFA concrete specimens.

Mix No.	Weight loss (%)	Compressive strength after the sulfate attack (MPa)	Compressive strength Reduction (%)
OPC	2.5	31.08	20.18
AM6	2.8	3.19	28.31
AL8	2.4	1.26	46.38
AM8	1.2	2.57	10.24
AH8	2.7	5.88	2.76
BM6	-1.4	15.46	-3.43
BL8	-0.7	13.55	5.86
BM8	-0.6	13.61	-7.84
BH8	-1.8	20.33	-12.01
CM6	-0.5	22.17	2.41
CL8	-1.3	39.33	-3.71
CM8	-1.8	37.82	-20.10
CH8	-1.8	41.76	-5.89
DM6	-1.4	34.11	-5.07
DL8	-1.2	53.67	-7.86
DM8	-2.1	55.18	-7.01
DH8	-2.3	57.64	-6.05
EM6	-1.6	43.85	-6.48
EL8	-1.9	59.29	-13.69
EM8	-1.4	56.78	-2.61
EH8	-1.3	60.37	-3.91

5. Scanning Electron Microscopy

To evaluate the effects of the FA/slag ratio, Na_2O concentration, and activator modulus ratio on the microstructure of the AAFS concrete specimens, SEM analysis was conducted,

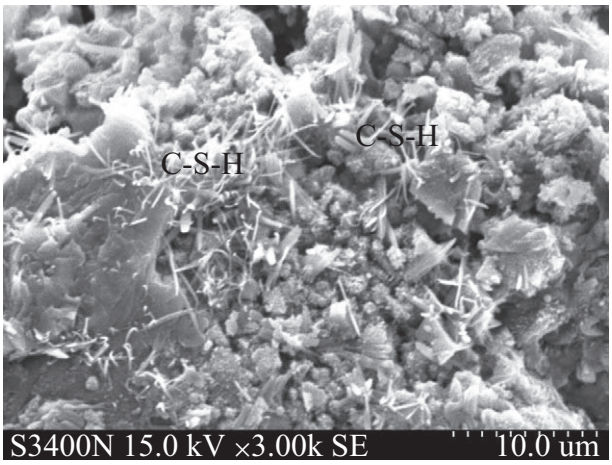

Fig. 11. SEM image of alkali-activated 100% slag-based concrete specimens with sodium oxide concentration of 6% and activator modulus ratio of 1 (EM6).

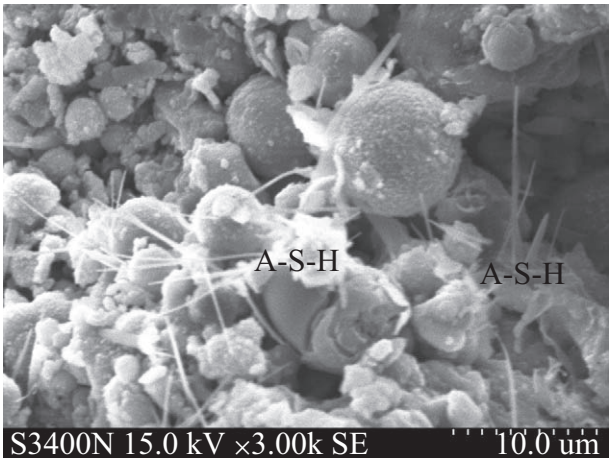

Fig. 12. SEM image of alkali-activated 100% fly ash-based concrete specimens with sodium oxide concentration of 8% and activator modulus ratio of 0.8 (AL8).

as shown in Figs. 11-13. The SEM images indicate that the EM6 concrete specimen (AAFS concrete with 100% slag-based binder) has a finer pore structure than that of the AL8 concrete specimen (AAFS concrete with 100% FA-based binder). The density of the composite matrix improved with increasing slag content. This may account for the increase in strength observed with the increasing amount of slag. Fig. 11 shows an SEM image of alkali-activated 100% slag-based concrete specimens with a Na_2O concentration of 6% and Na_2O/SiO_2 of 1.0 at 28 days. Some of the slag grains were totally hydrated, and the others were partially hydrated. The surface was darker because a rim of hydration products was deposited on the surface of the alkali-activated slag grains. Rod-like crystals of ettringite and C-S-H gel were the major hydration products, and they were localized in the area around the slag grains (Chi and Huang, 2013). The pores were filled with needle-like formations, and the main reaction product was C-S-H gel (Aydın and Baradan, 2012). Fig. 12 shows an SEM micrograph of the alkali-activated 100% FA-based concrete specimens with a Na_2O concentration of 8% and Na_2O/SiO_2 of 0.8 at 28 days. This figure indicates that FA geopolymers activated with sodium silicate form a heterogeneous material, containing both the completely reacted FA particles and partly reacted and unreacted FA particles covered with reaction products. On the spheres' surfaces, solid deposits or small crystals such as dendritic particles of iron minerals, soluble alkaline sulfates, and mullite crystals could be observed. In addition, quartz particles and vitreous unshaped fragments could be discerned. The precipitation of the reaction products forms a layer on the unreacted FA spheres, inhibiting their alkali activation (Fernández-Jiménez and Palomo, 2005). This may explain why the 100% FA-based concrete specimens without slag demonstrated extremely low compressive strength development. Fig. 13 depicts an SEM image representing the microstructure of the concrete specimens characterized by an alkali-activated FA/slag ratio of 50/50, Na_2O concentration of 6%, and Na_2O/SiO_2 ratio of 0.8. The main reaction products were a fully reacted matrix, partially reacted cenosphere, dense gel phase, and fibrous structure corresponding to C-S-H gel. In addition, a little aluminosilicate hydrate gel (A-S-H gel) could be observed.

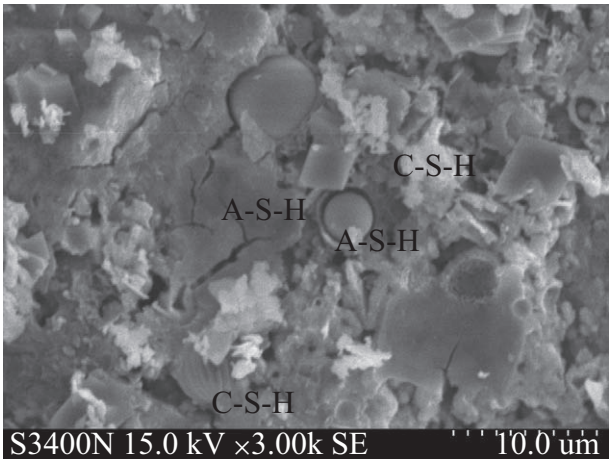

Fig. 13. SEM image of alkali-activated fly ash-to-slag ratio of 50/50 concrete specimens with sodium oxide concentration of 6% and activator modulus ratio of 0.8 (CL6).

The C-S-H and A-S-H gels coexisted in AAFS concrete, which is in agreement with the results of previous studies (Buchwald et al., 2007; Wang et al., 2012; Chi et al., 2015). Chemical interactions may arise between the elements released by the dissolution of FA and slag particles, and C-S-H and A-S-H may not be the only phases combined (Lloyd et al., 2009). The amount of slag added principally affected the amount of reaction product and its silicate structure. When the amount of slag added increased, the amount of C-S-H gel increased and the amount of aluminosilicate gel decreased (Lee and Lee, 2015).

IV. CONCLUSIONS

This study investigated the mechanical strength and durability of AAFS concrete specimens. Their performance was examined and compared with that of reference concrete produced using OPC. The following conclusions were drawn from the study:

1. The FA/slag ratio, activator modulus ratio, and Na_2O concentration considerably influence the mechanical strength and durability of AAFS concrete. The compressive strength of AAFS concrete also increases with slag content. Furthermore, higher activator modulus ratios and Na_2O concentration levels both improve the compressive strength of AAFS concrete. The trend in the splitting tensile strength of AAFS concrete is similar to that of its compressive strength.
2. The total charge passed through AAFS concrete is between 2500 and 4000 C, higher than that passed through the reference OPC concrete, but AAFS concrete demonstrates higher performance than that of OPC concrete when exposed to sulfate, in addition to exhibiting a certain increase in strength with time in sodium sulfate solution.
3. Alkali-activated 100% slag-based concrete has a finer pore structure than that of alkali-activated 100% FA-based concrete. For AAFS concrete with an FA/slag ratio of 50/50, C-S-H and A-S-H gels coexist in AAFS concrete.
4. According to the results, 100% slag-based AAFS concrete with a Na_2O concentration of 8% and activator modulus ratio of 1.23 offers superior performance.

ACKNOWLEDGMENTS

The author would like to thank the Ministry of Science and Technology (MOST) of Taiwan for Granting the Project under No. NSC-102-2221-E-274-007.

REFERENCES

ASTM C 39. (2014). Standard Test Method for Compressive Strength of Cylindrical Concrete Specimens. American Society for Testing and Materials.

ASTM C 88. (2013). Standard Test Method for Soundness of Aggregates by Use of Sodium Sulfate or Magnesium Sulfate. American Society for Testing and Materials.

ASTM C 150. (2012). Standard Specification for Portland Cement. American Society for Testing and Materials.

ASTM C 192. (2014). Standard Practice for Making and Curing Concrete Test Specimens in the Laboratory. American Society for Testing and Materials. Separation and Purification Technology.

ASTM C 496. (2011).Standard Test Method for Splitting Tensile Strength of Cylindrical Concrete Specimens. American Society for Testing and Materials.

ASTM C 618. (2012). Standard Specification for Coal Fly Ash and Raw or Calcined Natural Pozzolan for Use in Concrete. American Society for Testing and Materials.

ASTM C 1202. (2012). Standard Test Method for Electrical Indication of Concrete's Ability to Resist Chloride Ion Penetration. American Society for Testing and Materials.

Aydın, S. and B. Baradan (2012). Mechanical and microstructural properties of heat cured alkali-activated slag mortars. Materials and Design 35, 374-383.

Bakharev, T., J. G. Sanjayan and Y.-B. Cheng (1999). Alkali activation of Australian slag cements. Cement and Concrete Research 29, 113-120.

Bakharev, T., J. G. Sanjayan and Y.-B. Cheng (2002). Sulfate attack on alkali-activated slag concrete. Cement and Concrete Research 32, 211 -216.

Bernal, S., R. D. Gutierrez, S. Delvasto and E. Rodriguez (2010). Performance of an alkali-activated slag concrete reinforced with steel fibers. Construction and Building Materials 24, 208-214.

Bernal, S. A., R. M. d. Gutiérrez, A. L. Pedraza, J. L. Provis, E. D. Rodriguez and S. Delvasto (2011). Effect of binder content on the performance of alkali-activated slag concretes. Cement and Concrete Research (42), 1-8.

Bernal, S. A., R. M. d. Gutiérrez and J. L. Provis (2012). Engineering and durability properties of concretes based on alkali-activated granulated blast furnace slag/metakaolin blends. Construction and Building Materials 33, 99-108.

Buchwald, A., H. Hilbig and C. Kaps (2007). Alkali-activated metakaolin-slag blends-performance and structure in dependence of their composition. Journal of Material Science 42(9), 3024-3032.

Chi, M. (2012). Effects of dosage of alkali-activated solution and curing conditions on the properties and durability of alkali-activated slag concrete. Construction and Building Materials 35, 240-245.

Chi, M. and R. Huang (2012). Effects of Dosage and Modulus Ratio of Alkali-Activated Solution on the Properties of Slag Mortars. Advanced Science Letters 16(1), 7-12.

Chi, M. and R. Huang (2013). Binding mechanism and properties of alkali-activated fly ash/slag mortars. Construction and Building Materials 40, 291-298.

Chi, M., Y. Liu and R. Huang (2015). Mechanical and Microstructural Characterization of Alkali-Activated Materials Based on Fly Ash and Slag. IACSIT International Journal of Engineering and Technology 7(1), 59-64.

Collins, F. and J. G. Sanjayan (1999). Strength and shrinkage properties of alkali-activated slag concrete containing porous coarse aggregate. Cement and Concrete Research 29, 607-610.

Collins, F. and J. G. Sanjayan (2000). Cracking tendency of alkali-activated slag concrete subjected to restrained shrinkage. Cement and Concrete Research 30, 791-798.

Criado, M., A. F. Jiménez, I. Sobrados, A. Palomo and J. Sanz (2012). Effect of relative humidity on the reaction products of alkali activated fly ash. Journal of the European Ceramic Society 32, 2799-2807.

Duxson, P., A. Fernández-Jiménez, J. L. Provis, G. C. Lukey, A. Palomo and J. S. J. v. Deventer (2007). Geopolymer technology: the current state of the art. Journal of Materials Science 42(9), 2917-2933.

Duxson, P. and J. L. Provis (2008). Designing Precursors for Geopolymer Cements. Journal of the American Ceramic Society 91(12), 3864-3869.

Fernández-Jiménez, A., A. Palomo and M. Criado (2006). Alkali activated fly ash binders-A comparative study between sodium and potassium activators. Material Construction 56(281), 51-56.

Fernández-Jiménez, A., A. G. d. l. Torre, A. Palomo, G. López-Olmo, M. M. Alonso and M. A. G. Aranda (2006). Quantitative determination of phases in the alkali activation of fly ash. Part I. Potential ash reactivity. Fuel 85(5-6), 625-634.

Fernández-Jiménez, A. and A. Palomo (2005). Composition and microstructure of alkali activated fly ash binder: Effect of the activator. Cement and Concrete Research 35, 1984-1992.

Fernández-Jiménez, A., A. Palomo, I. Sobrados and J. Sanz (2006). The role played by the reactive alumina content in the alkaline activation of fly ashes. Microporous and Mesoporous Materials 91, 111-119.

Gao, X., Q. L. Yu and H. J. H. Brouwers (2015). Reaction kinetics, gel character and strength of ambient temperature cured alkali activated slag-fly ash blends. Construction and Building Materials, 80, 105-115.

Gruskovnjak, A., B. Lothenbach, L. Holzer, R. Figi and F. Winnefeld (2006). Hydration of alkali-activated slag: comparsion with ordinary Portland cement. Advanced Cement Research 18(3), 119-128.

Ismail, I., S. A. Bernal, J. L. Provis, R. S. Nicolas, S. Hamdan and J. S. J. v. Deventer (2014). Modification of phase evolution in alkali-activated blast

furnace slag by the incorporation of fly ash. Cement & Concrete Composites 45, 125-135.

Juengera, M. C. G., F. Winnefeldb, J. L. Provisc and J. H. Idekerd (2011). Advances in alternative cementitious binders. Cement and Concrete Research 41(12), 1232-1243.

Jun, Y. and J. E. Oh (2014). Mechanical and microstructural dissimilarities in alkali-activation for six Class F Korean fly ashes. Construction and Building Materials 52, 396-403.

Komljenović, M., Z. Baščarević and V. Bradić (2010). Mechanical and microstructural properties of alkali-activated fly ash geopolymers. Journal of Hazardous Materials 181, 35-42.

Komljenović, M., Z. Baščarević, N. Marjanović and V. Nikolić (2013). External sulfate attack on alkali-activated slag. Construction and Building Materials 49, 31-39.

Komljenović, M., Z. Baščarević, N. Marjanović and V. Nikolić (2013). External sulfate attack on alkali-activated slag. Construction and Building Materials, 49, 31-39.

Kumar, S., Kumar, R. and Mehrotra, S. P. (2009). Influence of granulated blast furnace slag on the reaction, structure and properties of fly ash based geopolymer. . Journal of Material Science, 45(3), 607-615.

Lee, N. K., J. G. Jang and H. K. Lee (2014). Shrinkage characteristics of alkali-activated fly ash/slag paste and mortar at early ages. Cement & Concrete Composites 53, 239-248.

Lee, N. K. and H. K. Lee (2013). Setting and mechanical properties of alkali-activated fly ash/slag concrete manufactured at room temperature. Construction and Building Materials 47, 1201-1209.

Lee, N. K. and H. K. Lee (2015). Reactivity and reaction products of alkali-activated, fly ash/slag paste. Construction and Building Materials 81, 303-312.

Lee, W. K. W. and J. S. J. v. Deventer (2002). The effect of ionic contaminants on the early-age properties of alkali-activated fly ash-based cements. Cement and Concrete Research 32(4), 577-584.

Li, C., H. Sun and L. Li (2010). A review: The comparison between alkali-activated slag (Si+Ca) and metakaolin (Si+Al) cements. Cement and Concrete Research 40, 1341-1349.

Lloyd, R., J. Provis and J. v. Deventer (2009). Microscopy and microanalysis of inorganic polymer cements. 2: the gel binder. Journal of Material Science 44(2), 620-631.

Lloyd, R. R., J. L. Provis and J. S. J. v. Deventer (2010). Pore solution composition and alkali diffusion in inorganic polymer cement. Cement and Concrete Research 40, 1386-1392.

Marjanović, N., M. Komljenović, Z. Baščarević, V. Nikolić and R. Petrović (2015). Physical-mechanical and microstructural properties of alkali-activated fly ash-blast furnaceslagblends. Ceramics International 41, 1421-1435.

Monteiro, P. J. M. and K. E. Kurtis (2003). Time to failure for concrete exposed to severe sulfate attack. Cement and Concrete Research 33(7), 987-993.

Neto, A. A. M., M. A. Cincotto and W. Repette (2008). Drying and autogenous shrinkage of pastes and mortars with activated slag cement. Cement and Concrete Research 38, 565-574.

Oh, J. E., P. J. M. Monteiro, S. S. Jun, S. Choi and S. M. Clark (2010). The evolution of strength and crystalline phases for alkali-activated ground blast furnace slag and fly ash-based geopolymers. Cement and Concrete Research, 40, 189-196.

Palomo, A., M. W. Grutzeck and M. T. Blanco (1999). Alkali-activated fly ashes: A cement for the future. Cement and Concrete Research 29, 1323-1329.

Phair, J., J. Deventer and J. Smith (2000). Mechanism of polysialation in the incorporation of zirconia into fly ash-based geopolymers. Industrial & Engineering Chemistry Research 39, 2925-2934.

Puertas, F., MartõÂnez-RamõÂrez, S., Alonso, S. and VaÂzquez, T. (2000). Alkali-activated fly ash/slag cement Strength behaviour and hydration products. Cement and Concrete Research, 30, 1625-1632.

Roy, D. M. (1999). Alkali-activated cements Opportunities and challenges. Cement and Concrete Research 29, 249-254.

Shi, C., A. F. Jiménez and A. Palomo (2011). New cements for the 21st century: The pursuit of an alternative to Portland cement. Cement and Concrete Research 41(7), 750-763.

Veiga, K. K. and A. L. G. Gastaldini (2012). Sulfate attack on a white Portland cement with activated slag. Construction and Building Materials, 34, 494-503.

Wang, J., X.-L. Wu, J.-x. Wang, C.-z. Liu, Y.-m. Lai, Z.-k. Hong and J.-p. Zheng (2012). Hydrothermal synthesis and characterization of alkali-activated slag-fly ash-metakaolin cementitious materials. Microporous and Mesoporous Materials 155(1), 186-191.

Yang, K.-H., J.-H. Mun, K.-S. Lee and J. Song (2011). Tests on cementless alkali-activated slag concrete using lightweight aggregates. International Journal of Concrete Structures and Materials 5(2), 125-131.

Yang, K.-H., J.-K. Song, A. F. Ashour and E.-T. Leed (2008). Properties of cementless mortars activated by sodium silicate. Construction and Building Materials, 22, 1981-1989.

Yang, T., X. Yao, Z. Zhang and H. Wang (2012a). Mechanical property and structure of alkali-activated fly ash and slag blends Journal of Sustainable Cement-Based Materials, (). pp. ISSN 2165-0373, 1(4), 167-178.

Yang, T., X. Yao, Z. Zhang and H. Wang (2012b). Mechanical property and structure of alkali-activated fly ash and slag blends. Journal of Sustainable Cement-Based Materials, 1(4), 167-178.

Zhao, F.-Q., W. Ni, H.-J. Wang and H.-J. Liu (2007). Activated fly ash/slag blended cement. Resources, Conservation and Recycling, 52, 303-313.

Zhu, H., Z. Zhang, Y. Zhu and L. Tian (2014). Durability of alkali-activated fly ash concrete: Chloride penetration in pastes and mortars. Construction and Building Materials 65, 51-59.